3652–3666 *Nucleic Acids Research, 2011, Vol. 39, No. 9* *Published online 17 January 2011*
doi:10.1093/nar/gkq980

PCNA directs type 2 RNase H activity on DNA replication and repair substrates

Doryen Bubeck[1], Martin A. M. Reijns[2], Stephen C. Graham[1], Katy R. Astell[2], E. Yvonne Jones[1] and Andrew P. Jackson[2,*]

[1]Division of Structural Biology, Wellcome Trust Centre for Human Genetics, University of Oxford, Oxford OX3 7BN and [2]Medical Research Council Human Genetics Unit, Institute of Genetics and Molecular Medicine, Western General Hospital, Edinburgh EH4 2XU, UK

Received July 15, 2010; Revised September 13, 2010; Accepted October 4, 2010

ABSTRACT

Ribonuclease H2 is the major nuclear enzyme degrading cellular RNA/DNA hybrids in eukaryotes and the sole nuclease known to be able to hydrolyze ribonucleotides misincorporated during genomic replication. Mutation in *RNASEH2* causes Aicardi–Goutières syndrome, an auto-inflammatory disorder that may arise from nucleic acid byproducts generated during DNA replication. Here, we report the crystal structures of *Archaeoglobus fulgidus* RNase HII in complex with PCNA, and human PCNA bound to a C-terminal peptide of RNASEH2B. In the archaeal structure, three binding modes are observed as the enzyme rotates about a flexible hinge while anchored to PCNA by its PIP-box motif. PCNA binding promotes RNase HII activity in a hinge-dependent manner. It enhances both cleavage of ribonucleotides misincorporated in DNA duplexes, and the comprehensive hydrolysis of RNA primers formed during Okazaki fragment maturation. In addition, PCNA imposes strand specificity on enzyme function, and by localizing RNase H2 and not RNase H1 to nuclear replication foci *in vivo* it ensures that RNase H2 is the dominant RNase H activity during nuclear replication. Our findings provide insights into how type 2 RNase H activity is directed during genome replication and repair, and suggest a mechanism by which RNase H2 may suppress generation of immunostimulatory nucleic acids.

INTRODUCTION

RNA/DNA hybrids form during many key cellular processes including DNA replication (1), transcription (2) and telomere elongation (3). Ribonuclease H (RNase H) endonucleases degrade the RNA strand of such RNA/DNA hybrids and therefore have a central importance in cellular physiology.

Eukaryotes have two classes of cellular RNase H enzymes: type 1 and 2 (4). RNase H1 (a type 1 enzyme) is essential for mitochondrial replication (5), while RNase H2 (a type 2 enzyme) is the predominant source of RNase H activity in mammalian cells (6). Despite low sequence similarity, both enzymes cleave at the 5′-end of RNA phosphodiester bonds using a highly conserved two metal ion catalytic mechanism (7–9). In addition, RNase H2 has the apparently unique ability to hydrolyze the 5′-phosphodiester bond of single ribonucleotides embedded in a DNA duplex (10,11).

Partial loss-of-function mutations in RNase H2 are a common cause of Aicardi–Goutières syndrome (AGS) (12,13). AGS is an auto-inflammatory genetic disorder that mimics *in utero* viral infection (14) and has immunological similarities to the autoimmune disease systemic lupus erythematosis (12,15). Inflammation is thought to be triggered by accumulating nucleic acid substrates that are normally degraded by cellular nucleases (16). Studies on TREX1, another nuclease mutated in AGS, have suggested that such nucleic acids may arise from recently replicated DNA (17), highlighting the need to understand the role of AGS nucleases in DNA replication.

During genomic DNA replication, synthesis on the lagging strand occurs discontinuously as Okazaki fragments. Synthesis is initiated by short RNA primers,

*To whom correspondence should be addressed. Tel: +44 131 332 2471; Fax: +44 131 343 2620; Email: andrew.jackson@hgu.mrc.ac.uk
Present address:
Stephen C. Graham, Cambridge Institute for Medical Research and Department of Clinical Biochemistry, University of Cambridge, Addenbrooke's Hospital, Hills Road, Cambridge CB2 0XY, UK.

The authors wish it to be known that, in their opinion, the first two authors should be regarded as joint First Authors.

on an average of 10 nt in length (18). During Okazaki fragment maturation these RNA primers are removed prior to fragment joining to form a continuous lagging strand. Several pathways for primer removal exist (19), and *in vitro* biochemical studies indicate that the sequential activities of RNase H2 and FEN1 may be involved (20–22). Additionally, as RNase H2 recognizes single ribonucleotides embedded in a DNA duplex, it is likely to have a role in DNA repair, facilitating removal of RNA bases misincorporated during genomic DNA replication (23). Recently, replicative DNA polymerases have been found to incorporate significant numbers of ribonucleotides during DNA synthesis (24), and so a role for RNase H2 in their removal may well be crucial to maintain genomic stability.

RNase H2 has been reported to interact with proliferating cell nuclear antigen (PCNA), although the functional consequences of this interaction were not established (25,26). PCNA assembles into a trimeric toroid (27) that clamps around double-stranded DNA. It acts both as a scaffold and catalyst for DNA-editing enzymes during DNA replication and repair (28). Many PCNA-interacting proteins bind a common hydrophobic groove near the PCNA C-terminus via a conserved peptide motif termed the PCNA interacting peptide (PIP) box motif (29,30). The PIP-box is defined by the sequence Qxxmxx$\Phi\Phi$ where x is any residue, m is aliphatic hydrophobic and Φ is an aromatic.

Archaeoglobus fulgidus (*Afu*) RNase HII is a single protein containing both the PIP-box (residues 199–205; QKTLDDF) and catalytic center, while the eukaryotic RNase H2 is a heterotrimeric complex with all three protein subunits required for enzymatic activity (11). The RNASEH2A subunit of the human enzyme contains the active site and forms a complex with the intimately interwoven RNASEH2B and RNASEH2C subunits (31). RNASEH2B possesses the PIP-box (residues 294–301; MKSIDTFF) which mediates its interaction with PCNA (26). The functional significance of this interaction between PCNA and type 2 RNase H is unclear as an inhibitory effect of PCNA on RNase HII enzymatic activity was seen in the thermophilic archaeon *Pyrococcus abyssi* (25) and no difference in human RNase H2 activity was observed in the presence of PCNA (26).

Given the potential roles of RNase H2 in genome replication and repair, and its relevance to autoimmune disease, we investigated the biological significance of the interaction between PCNA and type 2 RNase H. Here, we report the crystal structures of the *Afu* PCNA:RNase HII complex, as well as that of human PCNA bound to a peptide from human RNASEH2B. We establish the functional relevance of this interaction, demonstrating enhancement of RNase HII activity by PCNA both on ribonucleotides embedded within DNA and on Okazaki-like fragments. We also find that PCNA confers strand specificity to the enzyme's action. Finally, we demonstrate that RNase H2 is the only RNase H enzyme to localize to replication foci in mammalian cells through its interaction with PCNA, and suggest how it may suppress generation of inflammatory self nucleic acids.

MATERIALS AND METHODS

Cloning, expression and purification

Archaeoglobus fulgidus RNase HII and derivatives were expressed in Rossetta-2 using pGEX6P1-based vectors. Deletions and point mutations were introduced using the Quikchange method (Stratagene). *Archaeoglobus fulgidus* PCNA and human PCNA expression constructs were kind gifts from Professor J. Tainer (Scripps Research Institute) and Dr L. Cox (University of Oxford), respectively. For fluorescence microscopy *RNASEH2B* and *RNASEH2C* were cloned into pEGFP-C2-Dest, *RNASEH1* into pEGFP-N1. For details see Supplementary Table S1.

Cells were grown to OD_{600} 0.6 at 37°C and expression was induced with 1 mM IPTG for 3 h. Cells were pelleted and lysed by sonication in a PBS buffer containing 0.2% Tween, 10 mM $MgCl_2$, Protease Inhibitor Cocktail (Sigma; 50µl per gram of cell pellet) and 100 µg DNase I and 100 µg RNase A (Sigma; amounts per gram of cell pellet). GST-tagged proteins were bound to glutathione sepharose 4B beads, released by cleavage with PreScission protease (GE Healthcare Life Sciences) and further purified by size-exclusion chromatography in 150 mM NaCl, 20 mM Tris pH 7. Human and *Afu* PCNA were purified as previously described (27,32). *Archaeoglobus fulgidus* PCNA:RNase HII complex was separated from individual components by size-exclusion chromatography using a Superdex 200 column (GE Healthcare Life Science).

Crystallization, data collection and refinement

Crystals were grown by vapor diffusion at room temperature in 96-well plates with 0.2 µl drops. Equal volumes of pre-formed *Afu* PCNA:RNase HII complex (10 mg/ml in 150 mM NaCl, 20 mM Tris pH7) and precipitant (18% *w*/*v* PEG_{3350}, 196 mM K_2HPO_4 pH 9.2) were mixed. Crystals were cryoprotected with reservoir solution and 20% glycerol before cryocooling at 100 K. Diffraction data were collected at a wavelength of 1.00 Å at Diamond Light Source (Oxford, UK) at I04.

A peptide consisting of residues 290–312 from the RNASEH2B C-terminus (DKSGMKSIDTFFGVKNK KKIGKV; PIP-box motif underlined) was synthesized by solid phase synthesis, purified to >95% by reverse phase HPLC and freeze dried (Alta Bioscience). It was then rehydrated in 150 mM NaCl, 20 mM Tris pH7 and mixed with human PCNA (20 mg/ml) in equimolar amounts. Crystals grew in 3 M NaCl, 0.1 M citrate pH 3.5 and were dipped in perfluoropolyether PFO-X125/03 (Lancester Synthesis) before cryocooling. Diffraction data were collected at a wavelength of 0.982 Å at Diamond Light Source (Oxford, UK) at I03.

Data sets were integrated and scaled using HKL2000 (33) or CCP4/MOSFLM (34) scripted by Xia2 (35). Structures were determined by molecular replacement using Phaser (36) with *Afu* RNase HII (PDB ID: 1I39; residues 1–189) and *Afu* PCNA (PDB ID: 1RXM), or human PCNA (PDB ID: 1AXC) as search models. Models for the *Afu* RNase HII hinge and PIP-box and human RNASEH2B peptide were manually built using COOT (37). Models were initially refined with Phenix

(38) followed by further cycles with BUSTER-TNT (39) implementing 3-fold NCS restraints and TLS. Non-crystallographic local structure similarity restraints (40) were also used to deter deviation of the models from the target high-resolution *apo* RNase HII and PCNA crystal structures, unless evidence for a difference was present in the electron density. The geometry of the final refinement for both structures was assessed using MOLPROBITY (41). Of the residues in the *Afu* PCNA:RNase HII complex, 98.1% were in the favored region of the Ramachandran plot; none in the disallowed region. For the PCNA:peptide complex, 97.2% were in the favored region and 0.1% were outliers. All superpositions for structural analysis were done by secondary structure matching in COOT, unless otherwise indicated.

Modelling interaction with substrate

An RNA/DNA hybrid was modeled into the PCNA:RNase HII complex as previously described for murine RNase H2 (31). The RNA/DNA hybrid from the *Escherichia coli* RNase HI co-crystal structure (PDB ID: 1ZBI) was docked into the active site of *Afu* RNase HII based on the conserved metal coordination geometry between the two enzymes. As the *E. coli* structure was obtained using an RNase HI active site mutant (D132N), the positions of the furthest side chain carbon atoms were used as a proxy for the two oxygen atoms per active site residue that chelate the metal ions (*E. coli* RNase HI: CγD71, CγN132, CγD192; CδE109; *Afu* RNase HII: CγD6, CγD101, CγD129; CδE7). A least-squares fit of atoms from *E. coli* RNase HI on those from the three *Afu* RNase HII conformations was carried out using LSQ Superpose in COOT (37), independent of residue identity. The rotation and translation matrix generated was applied to the RNA/DNA hybrid (PDB ID: 1ZBI, chains A and B) using PDBSET in the CCP4 package (34). B-form DNA duplexes were generated in COOT and manually docked to continue the helix from the 5′-end of the hybrid through the PCNA ring. The hybrid and DNA duplex were joined after 10 cycles of idealization in REFMAC (42).

Co-precipitation experiments

Glutathione sepharose 4B beads with bound GST-RNase HII (1 μg) were mixed with non-tagged PCNA (0.4 μg) in NETN buffer (20 mM Tris pH 8, 100 mM NaCl, 1 mM EDTA, 0.5% NP-40) and incubated for 30 min at 4°C. Unbound proteins were collected and beads washed with buffer. Bound and unbound proteins were separated by SDS-PAGE (12%) and visualized with Coomassie stain.

To test for interactions of EGFP-RNASEH2B, transiently transfected COS7 cells were cross-linked for 30 min at 37°C with 0.25% formaldehyde, and cell lysates prepared as previously described (43). Proteins were captured with GFP-Trap beads as instructed by the manufacturer (Chromotek). Bound and unbound proteins were separated by SDS-PAGE and visualized by Western analysis using antibodies against GFP (JL8), PCNA (PC10), RNASEH2A and RNASEH2C.

RNase H activity assays

Ribonucleotide-containing oligonucleotides (^{32}P end-labeled) were annealed to unlabeled complementary DNA oligonucleotides (Supplementary Table S2 by heating for 5 min at 95°C and slow cooling to room temperature in 60 mM KCl, 50 mM Tris–HCl pH 8. Substrates and proteins were diluted in RNase H2 reaction buffer (50 mM Tris–HCl pH8, 60 mM KCl, 10 mM $MgCl_2$, 0.01% BSA and 0.01% Triton). Although the optimal growth temperature for *A. fulgidus* is 83°C, in keeping with previous studies (7,25), reactions were performed at 30°C. Reactions (5 μl) were incubated at 30°C for 20 min, unless otherwise indicated, and stopped by the addition of formamide loading dye. Samples were separated on 20% polyacrylamide (19:1, 1× TBE, 8 M urea) gels and bands were visualized by autoradiography.

Steady state enzyme kinetics

Experiments were performed using the conditions described by Chapados *et al.* (7) in the fluorescence-based enzyme assay described by Crow *et al.* (12) with 1 nM RNase HII and 1 μM PCNA at substrate concentrations ranging from 0 to 5 μM. Kinetic parameters K_m and V_{max} were determined using non-linear regression in SigmaPlot 11.0 (Systat Software Inc.).

Fluorescence microscopy

Transiently tranfected COS7 cells were fixed in 4% formaldehyde in PBS. Alternatively, cells were detergent extracted with 0.5% Triton X-100 in PBS for 5 min at room temperature, before fixing in 70% methanol-30% acetone (*v*/*v*) for 15 min at −20°C. For immunostaining, cells were blocked in 1% (*v*/*v*) fetal calf serum (FCS) in PBS, incubated with anti-PCNA antibody (PC10; Santa Cruz), washed in 1% FCS-PBS and incubated with secondary antibody (Alexa fluor 568; Invitrogen). Imaging was performed using a Coolsnap HQ CCD camera (Photometrics) and a Zeiss Axioplan II fluorescence microscope with Plan-neofluar objectives.

RESULTS

Crystal structure of the PCNA:RNase HII complex from *A. fulgidus*

The crystal structure of the *Afu* PCNA:RNase HII complex was solved by molecular replacement to 3Å resolution (Table 1). Three RNase HII molecules (23 kDa) bind the physiological PCNA homotrimer (81 kDa) (Figure 1 and Supplementary Figure S1). The primary interface is formed by the PIP-box motif of RNase HII that binds a hydrophobic groove proximal to the PCNA C-terminus. RNase HII rotates about a flexible hinge resulting in three distinct binding modes: two RNase HII molecules extend away from the ring, while the third occludes the central PCNA channel (Figure 1). Although portions of the RNase HII molecules are involved in crystal contacts, an analysis of the buried surface area using PISA (44) indicated that the contribution of

Table 1. Data collection and refinement statistics

	Afu PCNA:RNase HII	Human PCNA:RNASEH2B PIP
Data collection		
Space group	$P2_12_12$	$P2_1$
Cell dimensions		
a, *b*, *c* (Å)	149.7, 152.0, 90.2	83.1, 81.8, 116.6
α, β, γ (°)	90.0, 90.0, 90.0	90.0, 91.5, 90.0
Resolution (Å)	67.7–3.1 (3.13–3.05)[a]	47.5–3.0 (3.09–2.99)
R_{merge}	0.116 (1.086)	0.126 (0.852)
$I/\sigma I$	15.8 (2.0)	8.0 (1.8)
Completeness (%)	99.6 (96.6)	99.9 (99.9)
Redundancy	7.3 (7.2)	3.7 (3.8)
Refinement		
Resolution (Å)	67.7–3.1 (3.13–3.05)	47.5–3.0 (3.09–2.99)
No. of reflections	39 801 (2819)	31 807 (2930)
R_{xpct}[b]/R_{free}[c]	18.7 (25.8)/21.6 (30.4)	22.3 (25.9)/24.8 (28.3)
No. of atoms		
Protein	10 465	11 486
B-factors (Å^2)		
Protein	77.5	72.2
R.m.s. deviations		
Bond lengths (Å)	0.009	0.009
Bond angles (°)	1.08	1.09

[a]Values in parentheses are for highest-resolution shell.
[b]$R_{xpct} = 100 \times (\Sigma_{hkl} \; ||F_{obs}| - |F_{xpct}||/\Sigma_{hkl} \; |F_{obs}|)$, where $|F_{obs}|$ and $|F_{xpct}|$ are the observed structure facture amplitude and the expectation of the model structure factor amplitude, respectively (39).
[c]R_{free} was calculated from a randomly selected subset of the data, corresponding to 5%.

interfaces within the asymmetric unit (PCNA to RNase HII, PCNA to PCNA and RNase HII to RNase HII) are larger than of crystallographic contacts.

The *Afu* PCNA trimer in our crystal structure forms a closed ring with pseudo 6-fold symmetry. The core β-sheets comprise the outer circle while α-helices line the center of a toroid whose inner surface charge is complementary to a DNA duplex. This assembly is representative of the architecture observed for other PCNAs, irrespective of species and binding partner (27,45,46).

The previously reported structure of *apo Afu* RNase HII (7) revealed the protein to have an N-terminal globular domain (residues 1–157), consisting of a β-sheet flanked by α-helices, and a C-terminal helical cap (residues 158–200). In the active site, four catalytic residues (D6, E7, D101 and D129) chelate two metal ions. The core features of the unbound structure are preserved upon complex formation. Specifically, PCNA binding does not perturb the α/β fold of the N-terminal domain and the active site chemistry is conserved (Figure 2A). In the complex, the helical cap of RNase HII undergoes a conformational change, and as a result the extreme C-terminus becomes ordered, adopting a structure similar to that of the FEN1 C-terminus when bound to PCNA (45). Although it lacks the second aromatic residue of the consensus motif, the *Afu* RNase HII PIP-box still forms the 3_{10} helix that locks into the hydrophobic groove proximal to the PCNA C-terminus.

A flexible hinge region (residues 195–198) links the core of RNase HII with its PIP-box (residues 199–205) (Figure 2A). This hinge enables a wide range of motion of RNase HII relative to PCNA, three states of which are captured in the crystal structure. In the two extended conformations, the hinge is well ordered and makes additional contacts with PCNA (Figure 1A, B, C and F); while in the third conformation it is less ordered (Figure 1D). Notably, hinge residue RNase HII:R198, which immediately precedes the PIP-box, adopts a different conformation in each binding mode. In one heterodimer (Figure 1B) its side chain is extended, stabilizing the last residue of PCNA (S244). In addition, the guanidinium group of PCNA:R241 hydrogen bonds with the hydroxyl of RNase HII hinge residue S195. In the second heterodimer (Figure 1C), the side chain of RNase HII:R198 is folded back, disrupting the interaction between RNase HII:S195 and PCNA:R241. Consequently, PCNA:R241 forms a salt bridge with PCNA:D150. Significantly, the hinge could serve as a molecular switch to facilitate the transition between different binding modes of RNase HII.

We analyzed the range of motion between RNase HII and PCNA (Figure 1 and Supplementary Movie S1). Two of the three RNase HII molecules differ by only a 9° rotation, and their active sites lie at similar distances (46 Å and 49 Å, respectively) above the center of the ring (Figure 1B, C and E). The orientation of the third RNase HII molecule is remarkably different from the other two. Here, the core RNase HII domain is rotated a further 45°, capping one face of the ring and bringing the active site within 19 Å of the ring center (Figure 1D and E). In this binding mode, the N-terminal core domain of RNase HII makes additional contacts with a second PCNA monomer and substantially occludes the central channel. Given the more extensive interface and obstruction of the PCNA ring, this latter state may reflect an enzymatically inactive complex.

PCNA stimulates *Afu* RNase HII activity on physiologically relevant substrates

To assess the functional relevance of the interaction between *Afu* PCNA and RNase HII we examined the effect of PCNA on RNase HII activity *in vitro*. PCNA was found to stimulate the cleavage of a DNA duplex with a single embedded ribonucleotide (Figure 2C and D; data not shown). The specific activity for cleavage of $D_{14}R_1D_3$:D_{18} (250 nM) was 13-fold higher (13 ± 3; n = 4) in the presence of PCNA compared to RNase HII alone. This stimulation was dependent on the interaction of PCNA with RNase HII, as deletion of the RNase HII PIP-box abolished PCNA binding and enhancement of activity (Figure 2B and E). In contrast, deletion of the hinge region (ΔSNLR) permitted PCNA:RNase HII complex formation while still resulting in loss of PCNA stimulation (Figure 2B and F). Taken together, our data suggest that the hinge that permits the swinging movement of the RNase HII catalytic domain, is required for enzymatic action on substrates threaded through the PCNA ring.

Given the previous report of inhibition of archaeal RNase HII by PCNA (25), we next examined whether the effect of PCNA on RNase HII activity was position

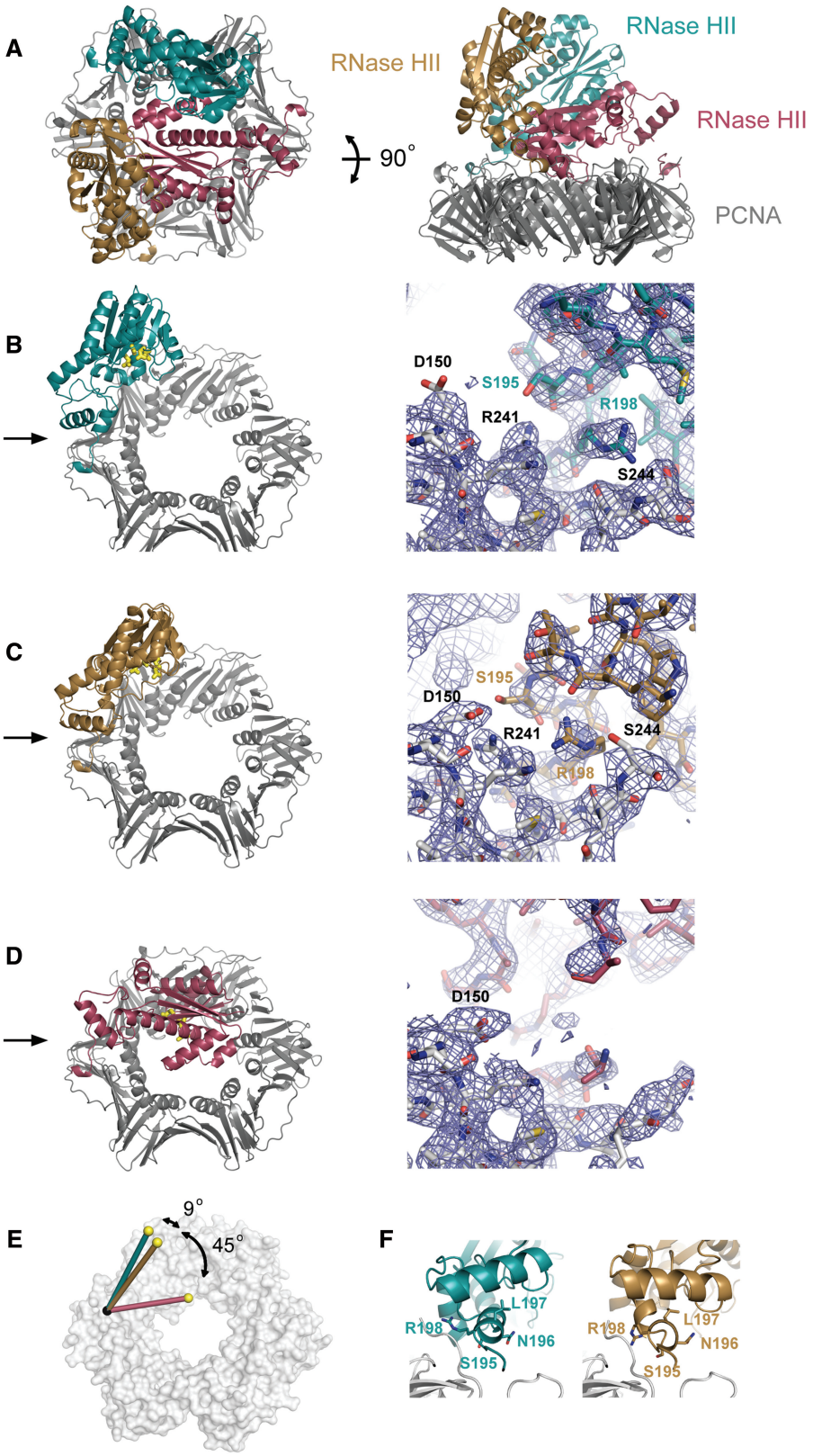

Figure 1. Structure of the *Afu* PCNA:RNase HII complex. (**A**) Three RNase HII molecules (cyan, tan and red) bind the PCNA homotrimeric ring (grey) in unique orientations. Two binding modes (cyan and tan) extend away from the center of the ring, while the third (red) obstructs the opening. On the right the complex is rotated 90° about the plane of the PCNA ring. (**B–D**) The three orientations of RNase HII observed in the complex with PCNA are shown independently from the same viewpoint. Active site residues (D6, E7, D101 and D129) are shown as yellow sticks. RNase HII is anchored to PCNA by its C-terminal PIP-box motif (residues 199–205) and rotates about a flexible hinge (black arrow). For each binding mode, a close-up of the hinge region (residues 195–198) reveals conformational changes in RNase HII and PCNA (right panel). PCNA residues R241, S244

(continued)

dependent. Enzymatic cleavage was assessed using substrates with a single ribonucleotide in different positions in the same 18 bp DNA duplex. Addition of PCNA had a stimulatory effect on cleavage when the RNA base was 12, 13, 14, 15 or 16 nt from the 5′-end of the substrate, (Figure 2D and Supplementary Figure S2F–H). In contrast, increasing the concentration of PCNA had a weak inhibitory effect when the RNA base was at positions 4, 6, 8 or 10 (Figure 2G and Supplementary Figure S2A–E). *Afu* RNase HII did not cleave at positions <4 bases from the 5′-end or <2 bases from the 3′-end, irrespective of the presence of PCNA (Supplementary Figure S2A and H and data not shown). A similar pattern was observed with longer substrates, with PCNA only stimulating cleavage at positions 3′ of base 10 (Supplementary Figure S2I–N). We therefore conclude that PCNA generally enhances enzymatic activity against single ribonucleotides embedded within a DNA duplex, unless the ribonucleotide is within the first ten 5′-bases of the strand containing it. This is consistent with the findings of Meslet-Cladière *et al*. (25) whose substrate contained a single ribonucleotide at position 8.

To establish whether these findings could be generalized for other type 2 RNase H substrates, we investigated enzymatic activity of PCNA:RNase HII on RNA/DNA heteroduplexes. A wide distribution of cleavage sites by RNase HII was observed and addition of PCNA enhanced cleavage (Supplementary Figure S3). PCNA also changed the cleavage pattern, inhibiting shorter cleavage products and shifting the preferred cleavage sites to generate fragments >12 nt in length. This is consistent with inhibition of cleavage for the first 10 nt. PCNA appears to enhance enzymatic activity by increasing effective substrate affinity, as stimulation was not observed at higher substrate concentration (Supplementary Figure S3B). Indeed, we show that substrate binding affinity is significantly higher in the presence of PCNA for both DNA duplex with a single embedded ribonucleotide and RNA/DNA heteroduplex substrate (Table 2).

To simulate unprocessed Okazaki fragments *in vitro*, we generated the substrate $D_{17}+R_{10}D_{13}$:D_{40}, which contains two oligonucleotides, D_{17} and $R_{10}D_{13}$ (mimicking the 5′- and 3′-ends of Okazaki fragments respectively) annealed to a 40 nt DNA strand (Figure 3A). Another substrate, $R_{10}D_{13}$:D_{40}, analogous to Primase-primed DNA, was generated in which only $R_{10}D_{13}$ was annealed to the 40 nt reverse strand. RNase HII alone preferentially cleaved at the phosphodiester bond 5′ of the junctional ribonucleotide, as previously described (47). In contrast, we observed more frequent cleavage at sites further away from the junction for substrate $D_{17}+R_{10}D_{13}$:D_{40} compared with $R_{10}D_{13}$:D_{40} (Figure 3B), suggesting that the presence of an upstream Okazaki fragment promotes more extensive hydrolysis of the RNA primer. We observed the same for human RNase H2 (Supplementary Figure S4). No cleavage of the single stranded $R_{10}D_{13}$ was observed for type 2 RNase H (*Afu*: Figure 3B; human: Supplementary Figure S4), indicating that the recombinant enzyme does not act as a junction ribonuclease on single stranded substrate, contrary to a previous report (47).

PCNA further enhanced cleavage of $D_{17}+R_{10}D_{13}$:D_{40} (Figure 3D and F), whereas it had no or very limited effect on the hydrolysis of $R_{10}D_{13}$:D_{40} that lacks the upstream 3′ Okazaki fragment (Figure 3C and E). This implies that the PCNA: RNase HII complex specifically enhances RNA primer degradation when synthesis of the upstream Okazaki fragment has been completed.

Additionally, PCNA:RNase HII appeared to generate smaller cleavage products with 5′-labeled substrate (Figure 3D). In contrast, PCNA enhanced cleavage of 3′-labeled substrate (Figure 3F) at the junctional ribonucleotide, without a significant change in the cleavage pattern. This is consistent with PCNA:RNase HII promoting increased catalysis at multiple sites rather than altering cleavage site preference, and could reflect increased RNase HII processivity when bound to PCNA.

Structural insights into the actions of the PCNA:RNase HII complex

To gain further insight into our biochemical findings, we modeled a nucleic acid substrate bound to the PCNA:RNase HII complex. Despite differences in sequence and secondary structure among RNase H enzymes, catalysis by two metals in the active site is conserved. Therefore, based on the geometry of the metal chelating atoms of *E. coli* RNase HI bound to an RNA/DNA hybrid (9), the substrate was modeled into active sites of two *Afu* RNase HII conformations (Figure 4). Docking resulted in the 5′-end of the RNA strand positioned proximal to the PCNA ring while the 3′-end passes through the substrate-binding region, as previously defined (7).

In our model, the RNA containing strand of the substrate threads from 5′- to 3′-through the center of the PCNA homotrimer to reach the active site and subsequent binding groove of RNase HII. The orientation of the binding groove within the context of the complex suggests that the role of the groove may not be to enhance substrate binding as was previously thought (8), but rather to distort the duplex geometry, facilitating cleavage. This is consistent with the inability of RNase HII to cleave ribonucleotides within 3 bases of the

Figure 1. Continued
and D150, and RNase HII residues S195 and R198 are labeled. The final refined model is shown in simulated annealing omit maps calculated for models in which residues corresponding to the hinge are removed (B, 3.0σ; C, 1.5σ; D, 4.0σ). (**E**) Schematic illustrating the range of motion between the three observed conformations. The hinge point (black sphere) marks the average Cα coordinate of PIP-box residue Q199. Cylinders are coloured according to the above models and yellow spheres highlight the average Cα coordinate of their respective active site residues. The PCNA ring is shown for reference (grey semi-transparent surface). (**F**) Close-up of the hinge region for the two RNase HII chains in which the entire sequence (^{195}SNLR^{198}) is resolved. These and all other molecular graphics were generated using PyMOL (DeLano Scientific LLC).

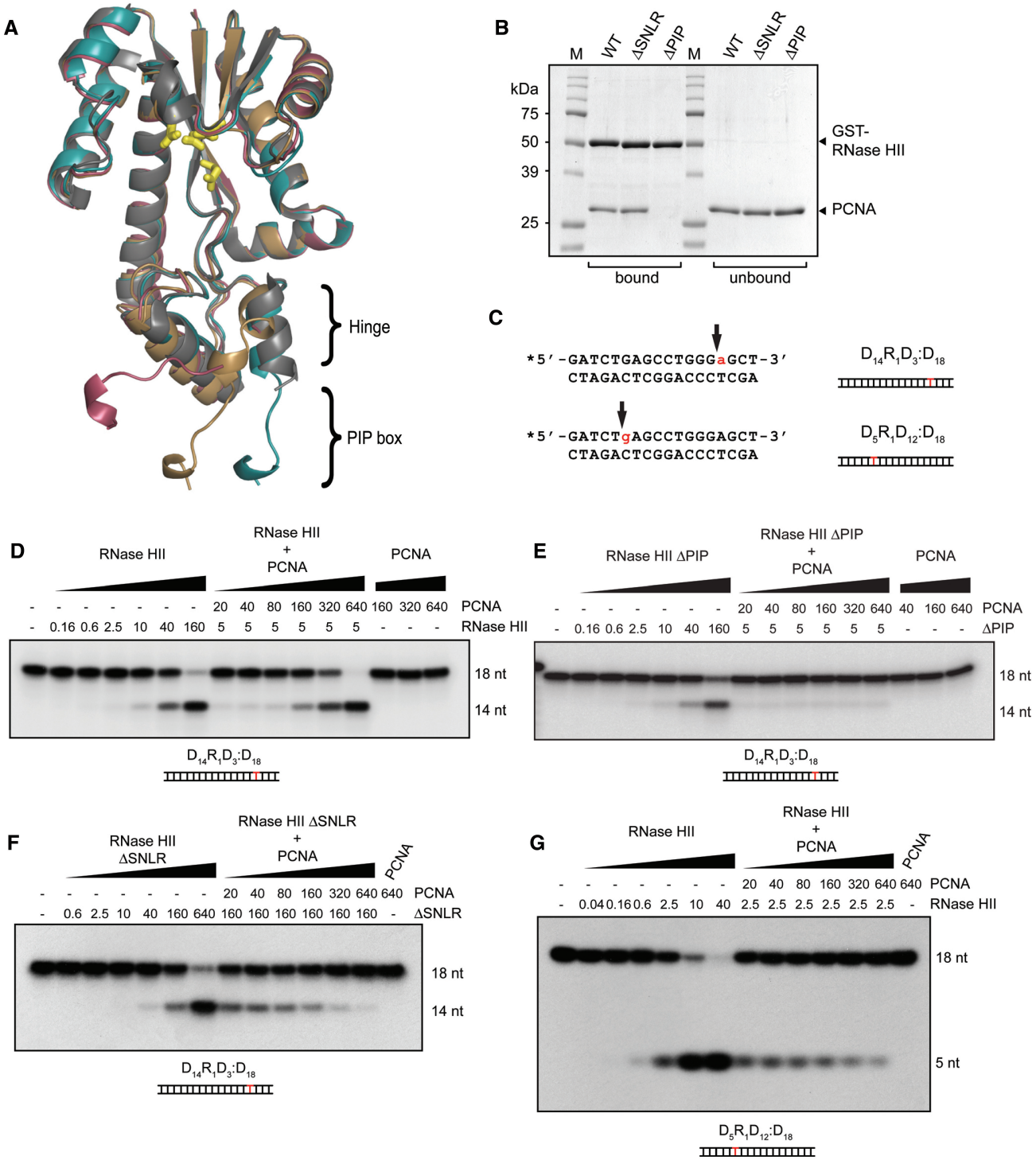

Figure 2. PCNA enhances RNase HII activity on certain substrates containing single ribonucleotides. (**A**) Superposition of the three RNase HII conformations (tan, cyan and red) with the *apo* RNase HII (grey) crystal structure (PDB ID: 1I39) highlighting the hinge region (residues $_{195}$SNLR$_{198}$) and PIP-box motif (residues $_{199}$QKTLDDF$_{205}$). Active sites residues are in yellow. (**B**) The RNase HII-PCNA interaction requires the PIP-box, but not the hinge region: GST-tagged wild-type, hinge deletion mutant (ΔSNLR), or PIP-box deletion mutant (ΔPIP) RNase HII was bound to glutathione beads and incubated with PCNA. Bound and unbound proteins were separated by SDS-PAGE and Coomassie stained. (M = Molecular weight marker) (**C**) Substrates used in panels **D–F** and **G**, respectively: 5′-labeled oligonucleotides (*) with a single ribonucleotide were annealed to a complementary DNA 18-mer. RNA bases in lower case (red); DNA bases in uppercase (black); cleavage positions indicated by arrows. (D) PCNA enhances RNase HII activity: Substrate $D_{14}R_1D_3$:D_{18} was incubated with *Afu* RNase HII and/or PCNA and separated by denaturing PAGE. (E) Enhancement of activity was lost when the RNase HII PIP-box was deleted (ΔPIP), (F) or when four hinge residues were removed (ΔSNLR). (G) PCNA inhibits RNase HII activity on substrate containing a ribonucleotide nearer the 5′-end ($D_5R_1D_{12}$:D_{18}). Contaminating nuclease activity in the recombinant proteins was excluded as neither PCNA alone, nor the RNase HII D101N active site mutant (data not shown) showed any substrate cleavage. All protein concentrations are indicated in nM; all assays were performed with 250 nM of substrate. Reactions incubated for 20 min at 30°C, except F (120 min).

Table 2. Kinetic parameters for Afu RNase HII in the absence and presence of PCNA

	K_m (μM)	k_{cat} (min^{-1})	k_{cat}/K_m ($min^{-1}\mu M^{-1}$)
$D_{14}R_1D_3$:DNA_{18}			
RNase HII	4.5 ± 2.3[a]	7.1 ± 3.0	1.6
RNase HII + PCNA	0.39 ± 0.16	3.3 ± 0.78	8.4
RNA_{18}:DNA_{18}			
RNase HII	2.4 ± 0.7	5.2 ± 1.5	2.1
RNase HII + PCNA	0.15 ± 0.07	0.96 ± 0.17	6.5

[a]Averages and standard deviations from four independent measurements.

3′-end of duplexes, even in the presence of PCNA (Supplementary Figure S2H).

To determine the relative position of the RNase HII catalytic site along the substrate, the docked hybrid was extended through the PCNA ring using a model for a B-form DNA duplex. The depth of the PCNA toroid is ~27 Å, equivalent to eight vertically stacked base pairs. In the crystal structure, the active sites of the RNase HII molecules are located 19.6, 46 and 49 Å from the center of the PCNA trimer, corresponding to ~6, 13 and 14 base pairs, respectively (Figure 4). For the two extended conformations the active sites lie within reach of RNA bases whose cleavage was stimulated by PCNA. However, for the third 'closed' conformation, substrate could not be modeled due to steric clashes and may represent an inhibitory state for the non-chromatin associated complex.

Our modeling shows that the catalytic site of RNase HII as part of the PCNA:RNase HII complex can access ribonucleotide bases distal to the 5′-end, but is physically obstructed from accessing those proximal, providing an explanation for the observed position-dependent PCNA activation and inhibition of RNase HII. Also implicit to this model is that PCNA confers strand specificity to the action of RNase HII, with enzymatic activity restricted to the strand passing 5′–3′ from the center of the PCNA ring to the catalytic site of the enzyme. This is supported by our biochemical data: In the absence of strand specificity, embedded ribonucleotides at positions 2–10 would be accessible to and cleaved by PCNA:RNase HII loaded from the opposite end, as PCNA rings can slide onto both ends of double stranded substrate in our *in vitro* system (48).

Structure of human PCNA with the RNASEH2B PIP-box peptide

Human RNase H2 is a complex of three subunits (RNASEH2A, RNASEH2B and RNASEH2C), all of which are required for activity. *Afu* RNase HII shares 29% sequence identity with the catalytic RNASEH2A subunit. However, it is the RNASEH2B subunit of the eukaryotic enzyme that contains the PCNA binding site (26). Therefore, to extend our observations for *Afu* PCNA:RNase HII to the corresponding human complex we solved the structure of a peptide from the C-terminus of human RNASEH2B bound to human PCNA to 3 Å resolution (Table 1, Figure 5A).

Twelve residues (DKSGMKSIDTFF) of the peptide were resolved in the final structure. Similar to *Afu*, the human RNASEH2B PIP-box interaction can be characterized by two distinct features: a 3_{10} helix that anchors into a hydrophobic pocket and a short stretch of amino acids N-terminal to the helix that form a β-sheet with the PCNA C-terminus (Figure 5B). Superposition of the PCNA components of human and *Afu* complexes demonstrates that the PIP-box structural motif is highly conserved through evolution (Figure 5C). The amide nitrogen of K6 and the carbonyl oxygen of G4 from the peptide hydrogen bond to the carbonyl oxygen of PCNA:P253 and the amide nitrogen of PCNA:I255, respectively, forming a β-zipper. This hydrogen-bonding pattern is conserved across many PCNA complexes (Supplementary Figure S5).

Recombinant PCNA by itself is not sufficient to stimulate human RNase H2 activity *in vitro*

As described above, we have shown enhanced activity for *Afu* PCNA:RNase HII; we therefore tested for cleavage of the same substrates by the human complex. However, we did not observe any effect of PCNA on recombinant human RNase H2 activity for any of these substrates (Supplementary Figure S4 and data not shown) over a range of reaction conditions. The human RNase H2 complex interacts with PCNA, as evident from gel filtration (26) and co-immunoprecipitation/co-localization experiments (Figure 6). However, we cannot exclude the possibility that the *in vitro* enzyme assay conditions are suboptimal for PCNA to bind the human enzyme and stimulate activity. Alternatively, given that our findings are consistent with the previously reported absence of stimulation (26), other factors may additionally regulate its activity. Regulatory post-translational modifications affecting enzyme activity have been demonstrated for other eukaryotic replication proteins (49). The presence of two additional subunits (RNASEH2B and RNASEH2C) in the eukaryotic enzyme also suggests the potential for further regulatory complexity through interactions with other proteins. Such regulation might be expected, permitting tight temporal and spatial control over RNase H2 activity.

Human RNase H2 but not RNase H1 localizes to replication foci

To confirm the physiological relevance of the human PCNA:RNase H2 complex, we investigated the interaction in a cellular context. We found EGFP-tagged human RNASEH2B to localize almost exclusively to the nucleus. Notably, 10–20% of transfected cells had punctate regions of higher intensity fluorescence within the nuclei, reminiscent of replication foci (Figure 6A). To further investigate this, cells were detergent extracted (Figure 6B), revealing EGFP-RNASEH2B co-localization

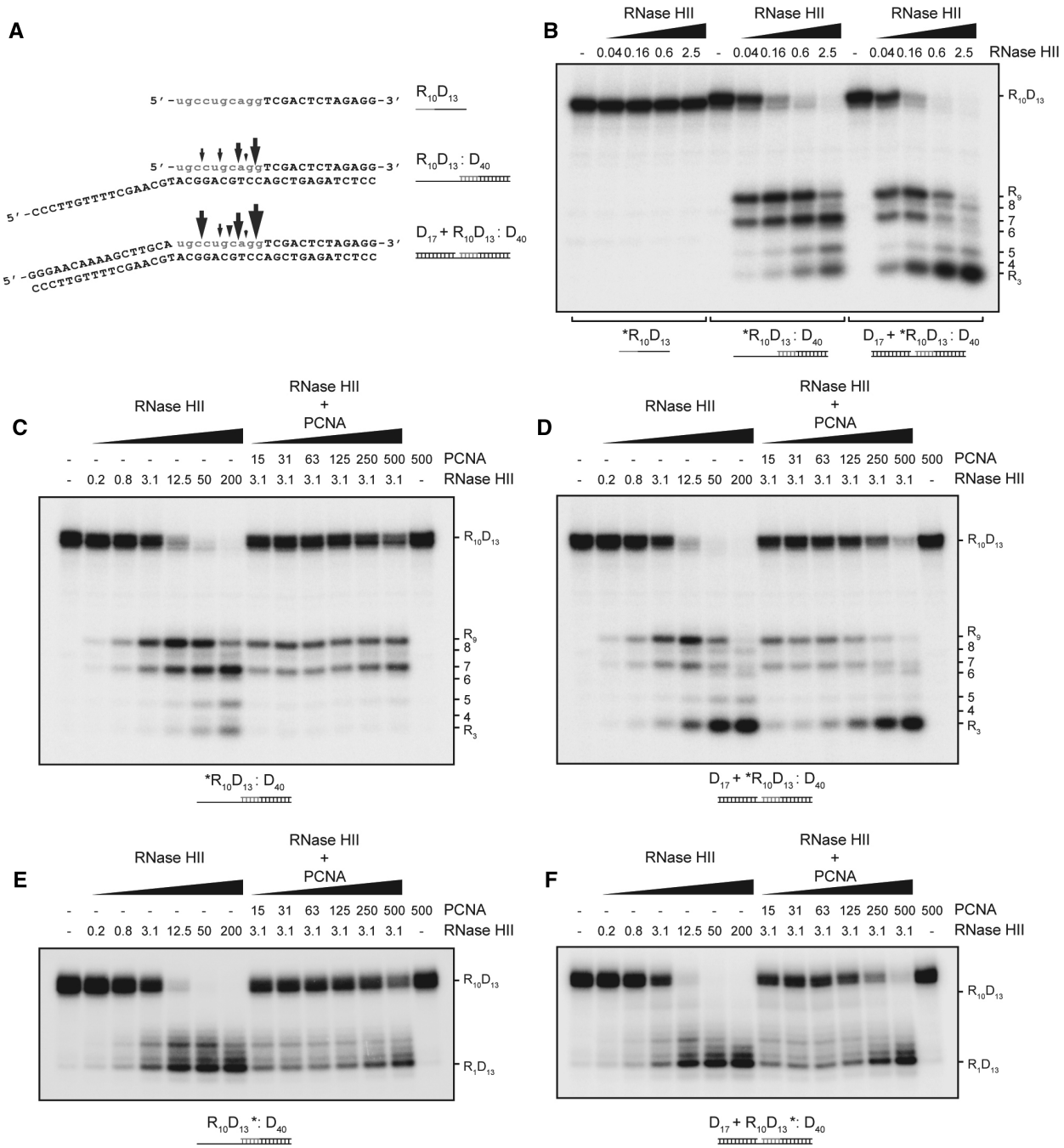

Figure 3. PCNA promotes efficient cleavage of Okazaki-like substrates by RNase HII. (**A**) Sequences of Okazaki-like fragments used in **B–F** (RNA bases in lower case, grey; DNA bases in upper case, black). $*R_{10}D_{13}$:D_{40} represents newly primed lagging strand DNA, while $D_{17}+*R_{10}D_{13}$:D_{40} corresponds to an unprocessed Okazaki junction. Arrows indicate cleavage sites with the size of the arrow indicating the extent of cleavage in the presence of PCNA. Each 5′-labeled substrate (2.5 nM) was incubated with *Afu* RNase HII and/or PCNA and separated by denaturing PAGE. (B) RNase HII generates smaller fragments from an unprocessed Okazaki junction. (C,D) PCNA enhances comprehensive cleavage of the RNA primer at a fully formed Okazaki junction, but not on primase-primed DNA. (E,F) 3′ labelling of $R_{10}D_{13}$ (0.5 nM) demonstrates that PCNA enhances cleavage at the junctional ribonucleotide of a fully formed Okazaki junction. All protein concentrations are given in nM. *In vitro Afu* PCNA homotrimer formation is inefficient at low concentrations, and consequently high concentrations of PCNA were used to supply sufficient PCNA trimeric rings for stimulation of RNase HII activity.

with non-extractable PCNA, which is a marker of sites of replication (50). EGFP-RNASEH2B was consistently present at replication foci in early-, mid- and late S-phase (Figure 6C and D), and its expression did not perturb cell cycle progression. Co-localization at replication was also seen for EGFP-RNASEH2C with PCNA, and RNASEH2B with EdU incorporated into newly synthesized DNA (Supplementary Figure S6).

Furthermore, RNASEH2B localization at replication foci could be disrupted by mutations in two phenylalanine

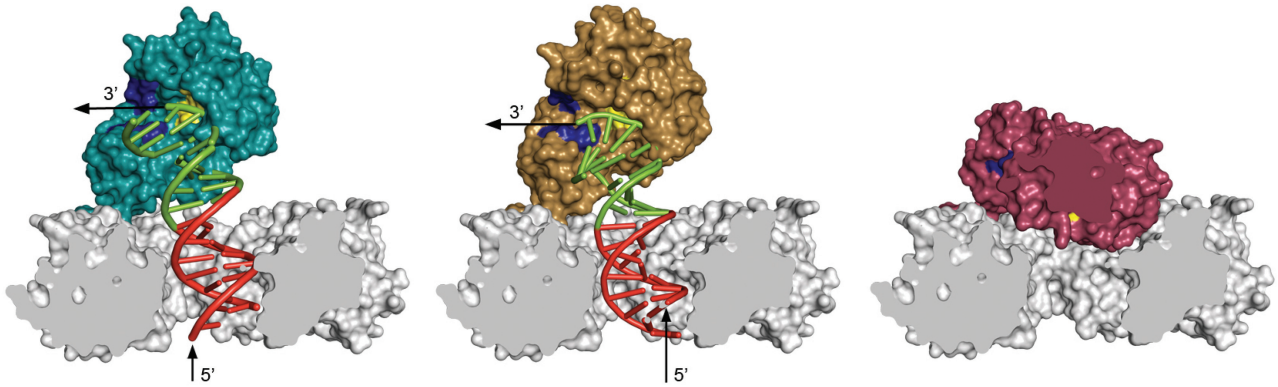

Figure 4. Model of RNA/DNA hybrid binding to the PCNA:RNase HII complex. An RNA/DNA hybrid was docked into the active site of *Afu* RNase HII, based on conserved metal coordination geometry (see 'Materials and Methods' section). The hybrid was extended through the PCNA ring with B-form DNA duplex. The three panels show molecular surfaces of the three RNase HII conformations (cyan, tan and red) from the same orientation on a single PCNA ring (grey). In the closed conformation (red), the duplex could not be modelled through the PCNA ring without significant steric clashes. The active site residues are shown in yellow and the binding groove (K143, R46, Q43, G161, S162, G163 and Y164) in blue. The color of bases along the RNA/DNA hybrid indicate the observed pattern of PCNA stimulation (green) and inhibition (red) on RNase HII cleavage. Arrows indicate the 5′- and 3′-ends of the RNA strand.

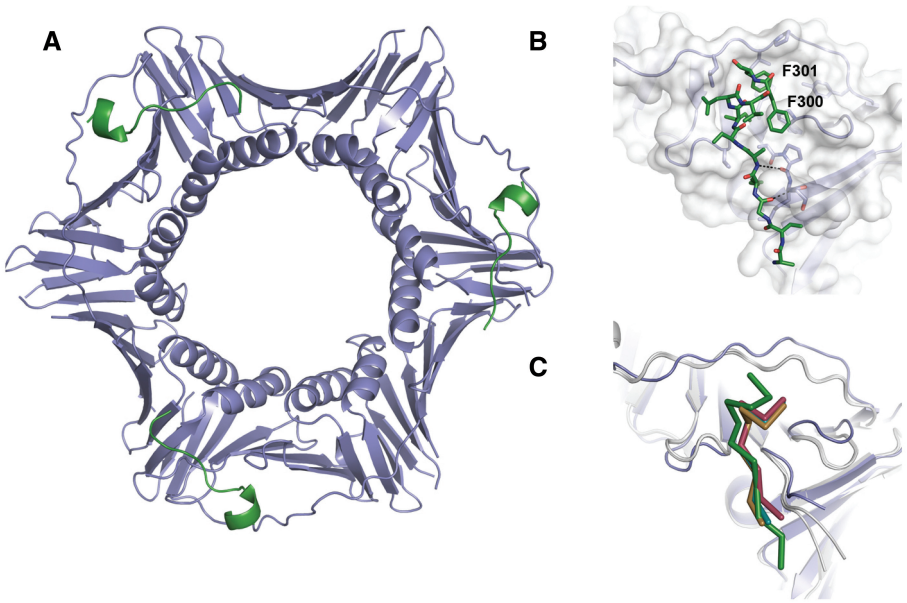

Figure 5. Crystal structure of a human PCNA:RNASEH2B PIP-box peptide complex. (**A**) A peptide corresponding to the C-terminal 18 residues of the RNASEH2B subunit (green ribbon) binds to each of the three PCNA monomers (light blue ribbon). (**B**) A view of the PIP-box interface shows the C-terminal component of the peptide (sticks, carbon atoms green) anchored into the hydrophobic pocket of PCNA (semi-transparent surface and light blue ribbon), while the N-terminal region forms hydrogen bonds (black dashes) with the backbone of the PCNA C-terminus. Residues F300 and F301 of RNASEH2B are labeled. Nitrogen and oxygen atoms in the interface are blue and red, respectively. (**C**) To compare Cα traces of the human RNASEH2B peptide (green) and the PIP-box of each of the *Afu* RNase HII conformations (cyan, tan and red), PCNA components of the *Afu* (grey ribbon) and human (light blue ribbon) complexes were superimposed.

residues of the PIP-box motif (Figure 5B; F300A and F301A), which are required for the interaction with PCNA (26) (Figure 6E). Although nuclear localization was unaltered, EGFP-RNASEH2B (FF > AA) (Figure 6A) no longer co-localized with PCNA after detergent extraction (Figure 6B). Therefore, the RNase H2 enzyme is targeted to replication factories through its PIP-box motif in the same manner as other replication enzymes (29). Notably, RNase H1 did not localize to replication foci at all (Figure 6A and B), so we conclude that in mammalian cells, RNase H2 is the ribonuclease H enzyme active at sites of replication.

DISCUSSION

Previous biochemical and genetic studies have suggested roles for RNase H activity in the removal of misincorporated ribonucleotides (23) and in Okazaki fragment maturation (20–22,51). We establish here that *Afu* PCNA enhances RNase HII activity on both these substrates, and

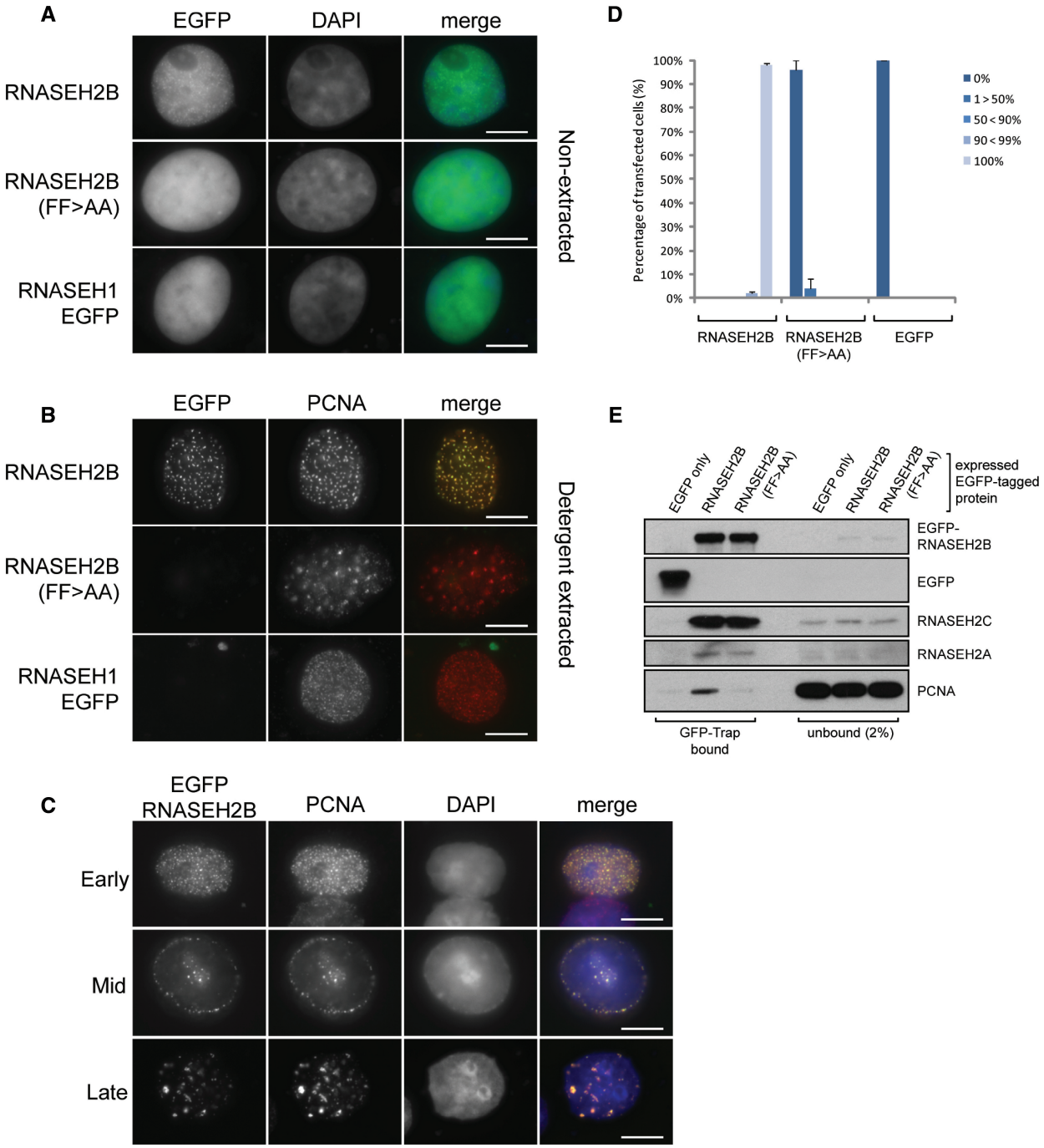

Figure 6. PCNA is sufficient to localize human RNase H2 to replication foci. (**A**) EGFP-RNASEH2B, the PIP-box mutant EGFP-RNASEH2B (FF > AA) and RNASEH1-EGFP (without mitochondrial localization signal) (5) localize to the nucleus in non-extracted COS7 cells. (**B**) Detergent extracted cells: EGFP-RNASEH2B requires an intact PIP-box to co-localize with PCNA at replication foci. RNASEH1-EGFP does not localize to replication foci. (**C**) EGFP-RNASEH2B co-localizes with PCNA through early-, mid- and late S-phase EGFP (green), PCNA (red), DAPI (blue); scale bars are 10 μm. (**D**) Quantification of co-localization between EGFP-RNASEH2B and PCNA in cells represented in panel B. Categories represent the percentage of foci with co-localizing signals in a cell. Graph shows average values of three independent experiments (100 cells per experiment); error bars indicate standard deviations. (**E**) RNase H2 interacts with PCNA in COS7 cells in a PIP-box dependent manner. EGFP proteins were affinity purified using GFP-Trap (Chromotek) from cell lysates. Bound/unbound proteins were detected by Western analysis.

that human PCNA localizes RNase H2, but not RNase H1, at replication foci. Therefore we conclude that type 2 RNase H in complex with PCNA provides the predominant RNaseH activity at sites of genome replication and repair. Our structural and biochemical data on the *Afu* PCNA:RNase HII complex also permit us to reassess previously proposed models and more clearly define how this enzyme acts in DNA replication and repair.

The role of PCNA:RNase H2 in removal of misincorporated ribonucleotides

Significant numbers of ribonucleotides are misincorporated during DNA synthesis by replicative DNA polymerases. Indeed, ribonucleotide bases may be present at a frequency of one in every few thousand base pairs of newly synthesized DNA. As DNA polymerases have difficulties bypassing these ribonucleotides in template DNA (24), a surveillance and repair mechanism that removes such ribonucleotides will be crucial to maintain genomic stability. Type 2 RNase H has the apparently unique ability to recognize and cleave single ribonucleotides embedded in DNA duplexes, making it a strong candidate for initiating such a process. Our demonstration that PCNA enhances RNase HII activity against such substrates suggests that this complex acts in this type of DNA repair, probably together with FEN1 which removes the ribonucleotide once a nick has been made (23). We therefore predict that PCNA:RNase H2 scans for misincorporated ribonucleotides in a processive strand-specific scanning mode, conferring increased efficiency over 3D diffusion that would be required for RNase H2 alone (Figure 7A).

PCNA directs type 2 RNase H enzymatic activity

The sequential action of RNase H2 and FEN1 could simply involve direct competition for the same PCNA binding site. However, a more interesting possibility is that they occupy two of the three available binding sites on the same PCNA trimer. PCNA would then coordinate their enzymatic activities, permitting substrate hand-off from one protein to the next. Structural modeling of a potential FEN1:PCNA:RNase HII complex demonstrates that this is possible, as the FEN1 and RNase HII hinges allow simultaneous binding without steric hindrance (Supplementary Figure S7). A similar coordinated transition from FEN1 to DNA ligase I has been suggested (52), and therefore this could represent a general mechanism for PCNA to facilitate sequential enzyme action. Conformations observed for other DNA-editing enzymes bound to a physiological PCNA ring have been suggested to reflect different activation states (45,53,54), but here we show a direct correlation between enzyme activity and conformation. Through biochemistry, utilizing ribonucleotides embedded at different substrate positions, and structural modeling of hybrids in the context of the complex, we infer that one state represents an inactive enzyme:PCNA complex, while two other orientations are enzymatically active forms. Furthermore, our experiments with embedded ribonucleotides allow us to demonstrate that PCNA confers strand specificity to RNase HII function that indeed may represent a general property for PCNA in the control of enzyme activities during replication and repair.

Models for PCNA:RNase H2 function in replication

The existence of multiple redundant pathways to deal with the discontinuous nature of lagging strand replication is generally assumed. Genetic studies in *Saccharomyces cerevisiae* suggest that RNase H2 acts in parallel with Rad27 (FEN1), Dna2 and Rad51 pathways in replication and repair (55,56). Although there is a significant case for a role of RNase H2 in Okazaki fragment processing, its precise function has remained elusive. Not least because RNase H2 is not an essential enzyme in *S. cerevisiae* and processing mechanisms involving flap generation have been highlighted in the recent literature (18,30). These mechanisms involve the displacement by Pol δ of a 5′–3′-flap of a downstream Okazaki fragment containing the RNA primer. This flap can be removed by the endonucleolytic activity of FEN1 or DNA2, without any

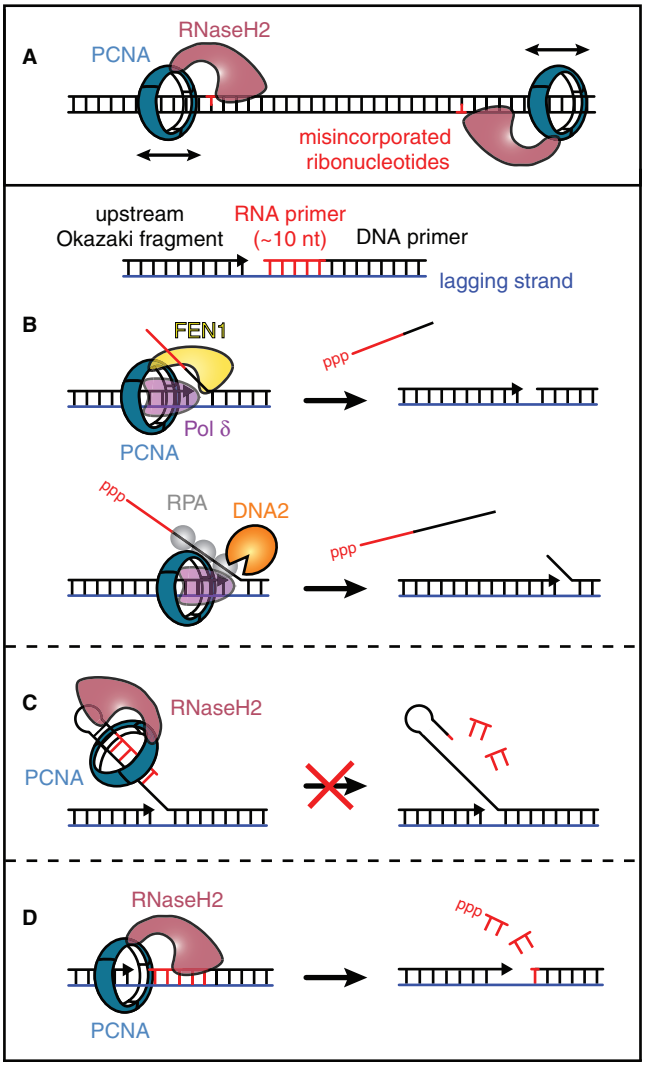

Figure 7. Models for PCNA:RNase H2 function in DNA repair and replication. (**A**) PCNA promotes type 2 RNase H recognition and cleavage of ribonucleotides that may become misincorporated during DNA synthesis. (**B**) Okazaki fragment maturation can occur through cleavage of 5′–3′-flaps by FEN1 or DNA2. Cleavage generates single stranded 5′-ppp RNA-DNA chimeras that have the potential to be highly immunogenic. (**C**) Fold-backs in raised flaps prevent resolution of these flaps by FEN1 (57). PCNA:RNase H2 cannot degrade the RNA primers in such hairpin structures, as PCNA obscures the primer. (**D**) PCNA:RNase H2 can efficiently remove RNA primers from Okazaki fragment junctions prior to flap generation by Pol δ, preventing formation of 5′-ppp nucleic acids.

requirement for RNase H activity (Figure 7B). However, FEN1 cleavage can be blocked if the strand folds back, forming a hairpin (57). RNase H2 has been proposed to play a role in processing these hairpin duplexes (58). However, our data indicate that the PCNA:RNase H2 complex cannot process such structures as the ribonucleotide containing strand must pass 5′–3′ through PCNA to reach the active site of RNase H2 (Figure 4). In the fold-back hairpins, the RNA primer would be masked by PCNA (Figure 7C).

Our data therefore favor RNase H2 acting on the RNA primer while it is still annealed to the lagging strand (Figure 7D). *In vitro* studies suggest that primer removal can be effected by RNase H2 cleavage of the primer, with the remaining ribonucleotide then removed by FEN1. Here we show that PCNA enhances RNase HII activity on Okazaki-like substrates in the presence of a completed upstream Okazaki fragment. PCNA:RNase HII also promotes more complete hydrolysis of the RNA primer, allowing ready dissociation of the resulting fragments. This is likely to be more energetically favorable than displacement of the intact primer by Pol δ in the form of a flap. Established mechanisms (18) that raise 5′–3′-flaps result in release of 5′-tri-phosphate nucleic acids (5′-pppRNA-DNA, Figure 7B). Unless degraded these could evoke an innate immune response: 5′-ppp nucleic acid species are potent agonists of intracellular pattern recognition receptors such as RIG-I (59,60). Primer degradation by PCNA:RNAse H2 prior to such flap generation would suppress the production of immunostimulatory 5′-ppp nucleic acids.

In summary, our findings provide important structural insights into how RNase H2 acts with PCNA to scan for misincorporated ribonucleotides and also rationalize the mechanisms by which this enzyme complex could act in Okazaki fragment processing. This will inform future biological investigations into the physiological functions of this enzyme and will be important in defining the nature and role of nucleic acids in the pathogenesis of systemic autoimmune disease.

ACCESSION NUMBERS

Atomic coordinates have been deposited at the RCSB protein data Bank under ID codes 3P83 for the *Afu* PCNA:RNase HII complex and 3P87 for the human PCNA:RNASEH2B peptide complex.

SUPPLEMENTARY DATA

Supplementary Data are available at NAR Online.

ACKNOWLEDGEMENTS

We are grateful to J. Ren, E. Mancini and K. Harlos for assistance in crystallographic data collection and refinement; to E. Freyer for help with fluorescence-activated cell sorting (FACS) analysis; to A. Leitch for generating antibody reagents; to J. Tainer and L. Cox for reagents and to T. Walter, E. Seiradake, B. Janssen, M. DiMattia, J. Caceres, N. Hastie, D. Stuart and members of the Jackson lab for useful discussions. We thank Diamond Light Source for synchrotron access.

FUNDING

Medical Research Council Senior Clinical Fellowship grant and Lister Institute of Preventative Medicine (to A.P.J.); Cancer Research UK grant (to E.Y.J.); Wellcome Trust Core Award (075491/Z04). European Molecular Biology Organization (EMBO), Cancer Research Institute (CRI) and St John's College (SJC) (to D.B.). Funding for open access charge: MRC Human Genetics Unit.

Conflict of interest statement. None declared.

REFERENCES

1. Machida,Y., Okazaki,T. and Okazaki,R. (1977) Discontinuous replication of replicative form DNA from bacteriophage phiX174. *Proc. Natl Acad. Sci. USA*, **74**, 2776–2779.
2. Li,X. and Manley,J.L. (2005) Inactivation of the SR protein splicing factor ASF/SF2 results in genomic instability. *Cell*, **122**, 365–378.
3. Forstemann,K. and Lingner,J. (2005) Telomerase limits the extent of base pairing between template RNA and telomeric DNA. *EMBO Rep.*, **6**, 361–366.
4. Ohtani,N., Haruki,M., Morikawa,M., Crouch,R., Itaya,M. and Kanaya,S. (1999) Identification of the genes encoding Mn2+-dependent RNase HII and Mg2+-dependent RNase HIII from Bacillus subtilis: classification of RNases H into three families. *Biochemistry*, **38**, 605–618.
5. Cerritelli,S.M., Frolova,E.G., Feng,C., Grinberg,A., Love,P.E. and Crouch,R.J. (2003) Failure to produce mitochondrial DNA results in embryonic lethality in Rnaseh1 null mice. *Mol. Cell*, **11**, 807–815.
6. Frank,P., Braunshofer-Reiter,C., Wintersberger,U., Grimm,R. and Büsen,W. (1998) Cloning of the cDNA encoding the large subunit of human RNase HI, a homologue of the prokaryotic RNase HII. *Proc. Natl Acad. Sci. USA*, **95**, 12872–12877.
7. Chapados,B.R., Chai,Q., Hosfield,D.J., Qiu,J., Shen,B. and Tainer,J.A. (2001) Structural biochemistry of a type 2 RNase H: RNA primer recognition and removal during DNA replication. *J. Mol. Biol.*, **307**, 541–556.
8. Chai,Q., Qiu,J., Chapados,B. and Shen,B. (2001) Archaeoglobus fulgidus RNase HII in DNA replication: enzymological functions and activity regulation via metal cofactors. *Biochem. Biophys. Res. Commun.*, **286**, 1073–1081.
9. Nowotny,M., Gaidamakov,S.A., Ghirlando,R., Cerritelli,S.M., Crouch,R.J. and Yang,W. (2007) Structure of human RNase H1 complexed with an RNA/DNA hybrid: insight into HIV reverse transcription. *Mol. Cell*, **28**, 264–276.
10. Eder,P.S. and Walder,J.A. (1991) Ribonuclease H from K562 human erythroleukemia cells. Purification, characterization, and substrate specificity. *J. Biol. Chem.*, **266**, 6472–6479.
11. Jeong,H.S., Backlund,P.S., Chen,H.C., Karavanov,A.A. and Crouch,R.J. (2004) RNase H2 of Saccharomyces cerevisiae is a complex of three proteins. *Nucleic Acids Res.*, **32**, 407–414.
12. Crow,Y., Leitch,A., Hayward,B., Garner,A., Parmar,R., Griffith,E., Ali,M., Semple,C., Aicardi,J., Babul-Hirji,R. *et al.* (2006) Mutations in genes encoding ribonuclease H2 subunits cause Aicardi-Goutières syndrome and mimic congenital viral brain infection. *Nat. Genet.*, **38**, 910–916.
13. Rice,G., Patrick,T., Parmar,R., Taylor,C.F., Aeby,A., Aicardi,J., Artuch,R., Montalto,S.A., Bacino,C.A., Barroso,B. *et al.* (2007) Clinical and molecular phenotype of Aicardi-Goutieres syndrome. *Am. J. Hum. Genet.*, **81**, 713–725.
14. Aicardi,J. and Goutieres,F. (1984) A progressive familial encephalopathy in infancy with calcifications of the basal ganglia

and chronic cerebrospinal fluid lymphocytosis. *Ann. Neurol.*, **15**, 49–54.
15. Ramantani,G., Kohlhase,J., Hertzberg,C., Innes,A.M., Engel,K., Hunger,S., Borozdin,W., Mah,J.K., Ungerath,K., Walkenhorst,H. *et al.* (2010) Expanding the phenotypic spectrum of lupus erythematosus in aicardi-goutieres syndrome. *Arthritis Rheum.*, **62**, 1469–1477.
16. Rigby,R.E., Leitch,A. and Jackson,A.P. (2008) Nucleic acid-mediated inflammatory diseases. *Bioessays*, **30**, 833–842.
17. Yang,Y., Lindahl,T. and Barnes,D. (2007) Trex1 exonuclease degrades ssDNA to prevent chronic checkpoint activation and autoimmune disease. *Cell*, **131**, 873–886.
18. Burgers,P.M. (2009) Polymerase dynamics at the eukaryotic DNA replication fork. *J. Biol. Chem.*, **284**, 4041–4045.
19. Rossi,M.L. and Bambara,R.A. (2006) Reconstituted Okazaki fragment processing indicates two pathways of primer removal. *J. Biol. Chem.*, **281**, 26051–26061.
20. Turchi,J., Huang,L., Murante,R., Kim,Y. and Bambara,R. (1994) Enzymatic completion of mammalian lagging-strand DNA replication. *Proc. Natl Acad. Sci. USA*, **91**, 9803–9807.
21. Goulian,M., Richards,S.H., Heard,C.J. and Bigsby,B.M. (1990) Discontinuous DNA synthesis by purified mammalian proteins. *J. Biol. Chem.*, **265**, 18461–18471.
22. Ishimi,Y., Claude,A., Bullock,P. and Hurwitz,J. (1988) Complete enzymatic synthesis of DNA containing the SV40 origin of replication. *J. Biol. Chem.*, **263**, 19723–19733.
23. Rydberg,B. and Game,J. (2002) Excision of misincorporated ribonucleotides in DNA by RNase H (type 2) and FEN-1 in cell-free extracts. *Proc. Natl Acad. Sci. USA*, **99**, 16654–16659.
24. Nick McElhinny,S.A., Watts,B.E., Kumar,D., Watt,D.L., Lundstrom,E.B., Burgers,P.M., Johansson,E., Chabes,A. and Kunkel,T.A. (2010) Abundant ribonucleotide incorporation into DNA by yeast replicative polymerases. *Proc. Natl Acad. Sci. USA*, **107**, 4949–4954.
25. Meslet-Cladiere,L., Norais,C., Kuhn,J., Briffotaux,J., Sloostra,J.W., Ferrari,E., Hubscher,U., Flament,D. and Myllykallio,H. (2007) A novel proteomic approach identifies new interaction partners for proliferating cell nuclear antigen. *J. Mol. Biol.*, **372**, 1137–1148.
26. Chon,H., Vassilev,A., DePamphilis,M., Zhao,Y., Zhang,J., Burgers,P., Crouch,R. and Cerritelli,S. (2009) Contributions of the two accessory subunits, RNASEH2B and RNASEH2C, to the activity and properties of the human RNase H2 complex. *Nucleic Acids Res.*, **37**, 96–110.
27. Gulbis,J.M., Kelman,Z., Hurwitz,J., O'Donnell,M. and Kuriyan,J. (1996) Structure of the C-terminal region of p21(WAF1/CIP1) complexed with human PCNA. *Cell*, **87**, 297–306.
28. Maga,G. and Hubscher,U. (2003) Proliferating cell nuclear antigen (PCNA): a dancer with many partners. *J. Cell. Sci.*, **116**, 3051–3060.
29. Montecucco,A., Rossi,R., Levin,D.S., Gary,R., Park,M.S., Motycka,T.A., Ciarrocchi,G., Villa,A., Biamonti,G. and Tomkinson,A.E. (1998) DNA ligase I is recruited to sites of DNA replication by an interaction with proliferating cell nuclear antigen: identification of a common targeting mechanism for the assembly of replication factories. *EMBO J.*, **17**, 3786–3795.
30. Garg,P. and Burgers,P.M. (2005) DNA polymerases that propagate the eukaryotic DNA replication fork. *Crit. Rev. Biochem. Mol. Biol.*, **40**, 115–128.
31. Shaban,N.M., Harvey,S., Perrino,F.W. and Hollis,T. (2010) The structure of the mammalian RNase H2 complex provides insight into RNA.NA hybrid processing to prevent immune dysfunction. *J. Biol. Chem.*, **285**, 3617–3624.
32. Hosfield,D.J., Mol,C.D., Shen,B. and Tainer,J.A. (1998) Structure of the DNA repair and replication endonuclease and exonuclease FEN-1: coupling DNA and PCNA binding to FEN-1 activity. *Cell*, **95**, 135–146.
33. Otwinowski,Z. and Minor,W. (1997) *Macromolecular Crystallography, Part A*. Academic Press, New York.
34. Collaborative Computational Project, Number 4. (1994) The CCP4 suite: programs for protein crystallography. *Acta Crystallogr. D Biol. Crystallogr.*, **50**, 760–763.
35. Winter,G. (2010) xia2: an expert system for macromolecular crystallography data reduction. *J. Appl. Crystallogr.*, **43**, 186–190.
36. McCoy,A.J., Grosse-Kunstleve,R.W., Storoni,L.C. and Read,R.J. (2005) Likelihood-enhanced fast translation functions. *Acta Crystallogr. D Biol. Crystallogr.*, **61**, 458–464.
37. Emsley,P. and Cowtan,K. (2004) Coot: model-building tools for molecular graphics. *Acta Crystallogr. D Biol. Crystallogr.*, **60**, 2126–2132.
38. Adams,P.D., Afonine,P.V., Bunkoczi,G., Chen,V.B., Davis,I.W., Echols,N., Headd,J.J., Hung,L.W., Kapral,G.J., Grosse-Kunstleve,R.W. *et al.* (2010) PHENIX: a comprehensive Python-based system for macromolecular structure solution. *Acta Crystallogr. D Biol. Crystallogr.*, **66**, 213–221.
39. Blanc,E., Roversi,P., Vonrhein,C., Flensburg,C., Lea,S.M. and Bricogne,G. (2004) Refinement of severely incomplete structures with maximum likelihood in BUSTER-TNT. *Acta Crystallogr. D Biol. Crystallogr.*, **60**, 2210–2221.
40. Smart,O., Brandl,M., Flensburg,C., Keller,P., Paciorek,W., Vonrhein,C., Womack,T. and Bricogne,G. (2008) Abstract TP139. *Annual Meeting of the ACA*, Knoxville, TN, 137.
41. Davis,I.W., Leaver-Fay,A., Chen,V.B., Block,J.N., Kapral,G.J., Wang,X., Murray,L.W., Arendall,W.B. III, Snoeyink,J., Richardson,J.S. *et al.* (2007) MolProbity: all-atom contacts and structure validation for proteins and nucleic acids. *Nucleic Acids Res.*, **35**, W375–W383.
42. Vagin,A.A., Steiner,R.A., Lebedev,A.A., Potterton,L., McNicholas,S., Long,F. and Murshudov,G.N. (2004) REFMAC5 dictionary: organization of prior chemical knowledge and guidelines for its use. *Acta Crystallogr. D Biol. Crystallogr.*, **60**, 2184–2195.
43. Gilljam,K.M., Feyzi,E., Aas,P.A., Sousa,M.M., Muller,R., Vagbo,C.B., Catterall,T.C., Liabakk,N.B., Slupphaug,G., Drablos,F. *et al.* (2009) Identification of a novel, widespread, and functionally important PCNA-binding motif. *J. Cell Biol.*, **186**, 645–654.
44. Krissinel,E. and Henrick,K. (2007) Inference of macromolecular assemblies from crystalline state. *J. Mol. Biol.*, **372**, 774–797.
45. Chapados,B., Hosfield,D., Han,S., Qiu,J., Yelent,B., Shen,B. and Tainer,J. (2004) Structural basis for FEN-1 substrate specificity and PCNA-mediated activation in DNA replication and repair. *Cell*, **116**, 39–50.
46. Sakurai,S., Kitano,K., Yamaguchi,H., Hamada,K., Okada,K., Fukuda,K., Uchida,M., Ohtsuka,E., Morioka,H. and Hakoshima,T. (2005) Structural basis for recruitment of human flap endonuclease 1 to PCNA. *EMBO J.*, **24**, 683–693.
47. Murante,R.S., Henricksen,L.A. and Bambara,R.A. (1998) Junction ribonuclease: an activity in Okazaki fragment processing. *Proc. Natl Acad. Sci. USA*, **95**, 2244–2249.
48. Burgers,P.M. and Yoder,B.L. (1993) ATP-independent loading of the proliferating cell nuclear antigen requires DNA ends. *J. Biol. Chem.*, **268**, 19923–19926.
49. Balakrishnan,L., Stewart,J., Polaczek,P., Campbell,J.L. and Bambara,R.A. (2010) Acetylation of Dna2 endonuclease/helicase and flap endonuclease 1 by p300 promotes DNA stability by creating long flap intermediates. *J. Biol. Chem.*, **285**, 4398–4404.
50. Leonhardt,H., Rahn,H.P., Weinzierl,P., Sporbert,A., Cremer,T., Zink,D. and Cardoso,M.C. (2000) Dynamics of DNA replication factories in living cells. *J. Cell. Biol.*, **149**, 271–280.
51. Qiu,J., Qian,Y., Frank,P., Wintersberger,U. and Shen,B. (1999) Saccharomyces cerevisiae RNase H(35) functions in RNA primer removal during lagging-strand DNA synthesis, most efficiently in cooperation with Rad27 nuclease. *Mol. Cell. Biol.*, **19**, 8361–8371.
52. Mayanagi,K., Kiyonari,S., Saito,M., Shirai,T., Ishino,Y. and Morikawa,K. (2009) Mechanism of replication machinery assembly as revealed by the DNA ligase-PCNA-DNA complex architecture. *Proc. Natl Acad. Sci. USA*, **106**, 4647–4652.
53. Doré,A.S., Kilkenny,M.L., Jones,S.A., Oliver,A.W., Roe,S.M., Bell,S.D. and Pearl,L.H. (2006) Structure of an archaeal PCNA1-PCNA2-FEN1 complex: elucidating PCNA subunit and client enzyme specificity. *Nucleic Acids Res.*, **34**, 4515–4526.

54. Bowman,G.D., O'Donnell,M. and Kuriyan,J. (2004) Structural analysis of a eukaryotic sliding DNA clamp-clamp loader complex. *Nature*, **429**, 724–730.
55. Ii,M. and Brill,S.J. (2005) Roles of SGS1, MUS81, and RAD51 in the repair of lagging-strand replication defects in Saccharomyces cerevisiae. *Curr. Genet.*, **48**, 213–225.
56. Chen,J.Z., Qiu,J., Shen,B. and Holmquist,G.P. (2000) Mutational spectrum analysis of RNase H(35) deficient Saccharomyces cerevisiae using fluorescence-based directed termination PCR. *Nucleic Acids Res.*, **28**, 3649–3656.
57. Henricksen,L.A., Tom,S., Liu,Y. and Bambara,R.A. (2000) Inhibition of flap endonuclease 1 by flap secondary structure and relevance to repeat sequence expansion. *J. Biol. Chem.*, **275**, 16420–16427.
58. Kao,H.I. and Bambara,R.A. (2003) The protein components and mechanism of eukaryotic Okazaki fragment maturation. *Crit. Rev. Biochem. Mol. Biol.*, **38**, 433–452.
59. Schlee,M., Hartmann,E., Coch,C., Wimmenauer,V., Janke,M., Barchet,W. and Hartmann,G. (2009) Approaching the RNA ligand for RIG-I? *Immunol. Rev.*, **227**, 66–74.
60. Rehwinkel,J. and Reis e Sousa,C. (2010) RIGorous detection: exposing virus through RNA sensing. *Science*, **327**, 284–286.